CardioFi: Enabling Heart Rate Monitoring on Unmodified COTS WiFi Devices

Abdelwahed Khamis
UNSW, Sydney, Australia
Data61, CSIRO, Sydney, Australia
a.khamiss@student.unsw.edu.au

Chun Tung Chou
UNSW, Sydney, Australia
c.t.chou@unsw.edu.au

Branislav Kusy
Data61, CSIRO, Brisbane, Australia
brano.kusy@data61.csiro.au

Wen Hu
UNSW, Sydney, Australia
Data61, CSIRO, Sydney, Australia
wen.hu@unsw.edu.au

ABSTRACT

Heart rate is one of the most important vital signals for personal health tracking. A number of approaches were proposed to monitor heart rate, ranging from wearables to device-less systems. While WiFi has been shown to track heart rate accurately, existing solutions rely on directional antennas to improve the signal quality and ultimately the accuracy of heart rate estimation. Special hardware used in these approaches limits their applicability and truly device-less and ubiquitous heart rate monitoring is yet to be achieved.

In this paper, we propose CardioFi: a system that can accurately monitor vital signs through COTS WiFi hardware with omni-directional antennas. Our key challenge is the substantial radio frequency noise that affects WiFi transmissions in real-world environments. However, we observe that a few sub-carriers are typically less affected by multipath and the heart beating motion can be accurately detected in their frequency spectrum. We present a novel sub-carrier selection scheme that allows us to detect and amplify signal from these sub-carriers even in low signal-to-noise ratio scenarios. We show that CardioFi estimates heart rate with 1.1 beats per minute (bpm) median error, which compares favorably with systems equipped with directional antennas. Furthermore, we show that state-of-art heart rate estimation algorithms do not perform well in low SNR scenarios and CardioFi improves their 50- and 90-th percentile error by 40% and 176%, respectively.

CCS CONCEPTS

• **Human-centered computing** → **Ubiquitous and mobile computing**;

KEYWORDS

WiFi Sensing, device-free, CSI, heart rate

1 INTRODUCTION

Ubiquitous health monitoring had witnessed a surge of interest in the past few years. Current heart rate monitoring solutions mostly employ wearable devices attached to the user's body. The alternative device-free heart rate monitoring offers improvements in comfort, ease of use, and does not require close cooperation of the subject, which are important aspects especially in the health care context. Commodity WiFi devices have recently been used for contact-free monitoring of vital signs, such as heartbeat and respiration [14, 28].

While demonstrating promising performance for respiration monitoring, commodity WiFi technology requires directional antennas to achieve accurate heart rate monitoring. The key observation is that directional antennas help to substantially reduce multipath effects in complex real-world environments that render signals obtained with omnidirectional antennas difficult to analyze. In addition to respiration and heartbeat monitoring, directional WiFi antennas have enabled new sensing modalities, such as lip reading [26], WiFi imaging [12], and gesture recognition [17].

The key question we ask in this paper is: *Is it possible to accurately monitor heartbeat of a person using ubiquitous consumer RF devices that are not attached to the person?* We show the positive answer to this by designing, implementing, and validating a system comprised of Commercial Off-The-Shelf (COTS) WiFi devices that track instantaneous heartbeat of a person with median accuracy of 1.1 beats per minute.

Unlike previous research, we consider a specific scenario with two devices communicating over WiFi near a user. The two devices can be, for example, a laptop and a portable device both using built-in omni-directional antennas and one of the devices collects channel state information (CSI) data associated with WiFi transmissions. Our key observation is that despite the substantial noise present in the CSI signals, the impact of the noise on individual sub-carriers is frequency dependent. Specifically, several sub-carriers typically

contain strong heartbeat frequency related frequency components and are sufficient for making accurate heartbeat estimation.

Based on our observation, we implement filtering and sub-carrier selection algorithms that rank the sub-carriers according to their heartbeat information content. Related work has primarily adopted the variance-based selection method that discards sub-carriers with low variance [14, 27, 28] or ranked sub-carriers according to their periodicity [16]. While these approaches tend to work well when the motion level is sufficiently strong to modulate the amplitude of the received signal (such as breathing, walking), they fail when the motion is weak and easily dominated by other environmental RF noise. Through experiments, we show that existing methods yield noisy frequency curves and significant energy peaks at frequencies distributed across the whole heartbeat frequency spectrum. Our sub-carrier selection method takes advantage of the spectral history and chooses those sub-carriers with consistent dominant frequency component over a specified time window.

We make the following contributions in this paper:

- We demonstrate the *feasibility of contact-less extraction of heart rate from Channel State Information (CSI) of COTS WiFi devices* without extra hardware such as directional antennas. This is to the best of our knowledge, the first system that does not rely on bulky directional antennas. The proposed approach estimates the heart rates with median error comparable to directional antennas for user-to-apparatus distances of up to 2 meters and shows an improvement of 40% compared to previous work [14].
- We propose a *novel sub-carrier ranking scheme* based on Spectral Stability, which is capable of selecting informative sub-carriers in situations where the majority of the sub-carriers are noisy. The scheme leverages the known frequency range of the heart beating and is computationally efficient, which makes it suitable for instantaneous heart rate estimation. The proposed scheme reduces the median error by 19% compared to previous sub-carrier selection approaches based on variance.

The rest of this paper is organized as follows. We start by motivating the problem of WiFi-based contact-free heart rate estimation in the absence of bulky directional antennas in Section 2, where we also highlight the challenges and our observations for making the heart rate estimation possible. Next in Section 3, we show the proposed CardioFi system architecture. Then, in Section 4, we evaluate the system's performance and study the impact of different parameters, which is followed by the overview of related works in Section 5. Finally, we conclude the paper in Section 6.

2 MOTIVATION

The state of a wireless channel is affected by the movement of people and objects in the transmission medium. For WiFi devices, these movements induce changes in the CSI of different sub-carriers. The key idea behind WiFi sensing is to use the CSI to infer the movements that have caused the changes in CSI. By using this inference, researchers have been able to successfully perform location tracking [32], gesture recognition [23], breathing rate estimation [29, 34], gait [33] and many other applications.
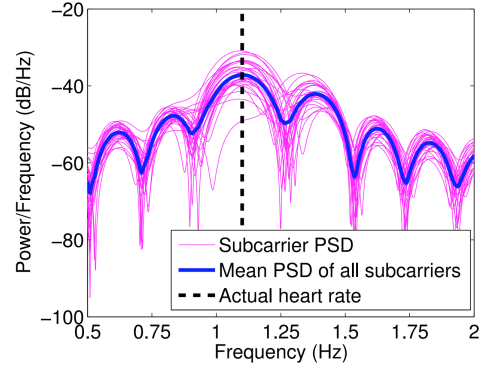

(a) Directional antennas
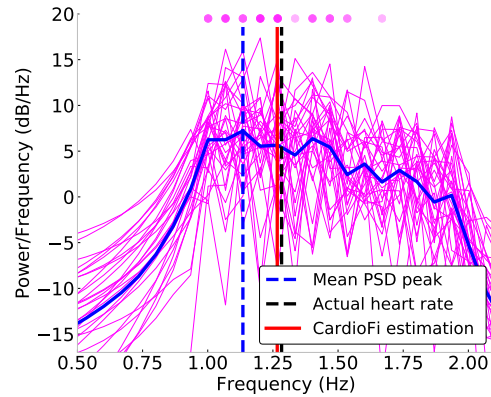
(b) Commodity WiFi antennas

Figure 1: PSD curves for CSI data collected using: (a) directional ([14]) and (b) omni-directional antennas. The low SNR in (b) makes the heart rate estimation a challenge.

Our aim is to use COTS WiFi devices to estimate the heart rates. Although the estimation of breathing rate from CSI data has already been demonstrated [29, 34], it is challenging to estimate the heart rate from CSI data because the heart movement is significantly smaller in magnitude compared to that of the lungs. The chest movement due to breathing is approximately 4-12 mm [7] and causes a periodic variation in the CSI time series which is easily discernible by naked eyes. However, the chest movement due to the heart is an order of magnitude smaller, at approximately 0.2-0.5 mm [21], and can only induce a small change in CSI.

The mixing of the movement due to breathing and the heart can cause another problem. Since breathing movement is lower in frequency than that of the heart, the higher harmonics due to breathing can interfere with the signal due to the heart [20, 28].

In order to overcome these challenges, Liu et. al. employed frequency analysis to isolate the heart rate frequency band from that of breathing, and used **directional antenna** to boost the signal's quality [14]. Fig. 1(a) (presented as Fig.8(b) in [14]) shows the results. The thin magenta lines in the figure show the Power Spectral
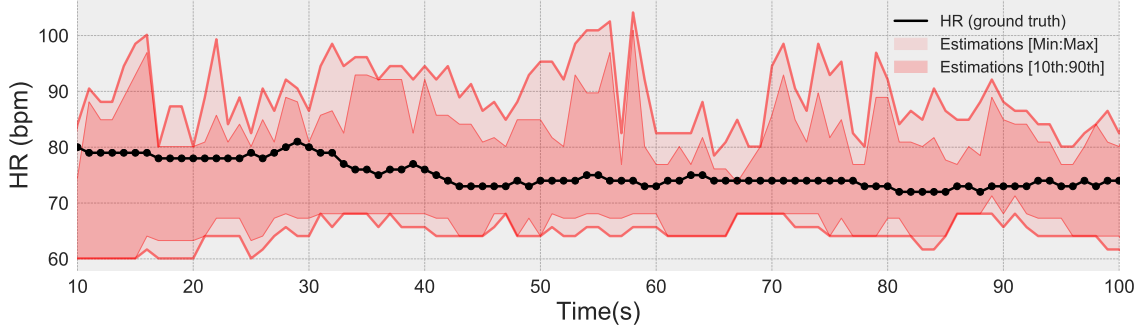
Figure 2: Actual heart rate compared to the estimation produced from individual sub-carriers. At each point in time, different sub-carriers produce estimation that varies largely (illustrated by the red shaded areas whose boundary represent maximum and minimum estimation at that point). Even after discarding extreme estimates (darker area), the range continues to be large.

Density (PSD) of the amplitude of the CSI time series from different sub-carriers after filtering out the frequency range in which the heart rates are unlikely to be found. The thick blue line shows the mean PSD of all the sub-carriers, which shows a distinct peak at a frequency very close to the actual heart rate indicated by the black dashed lines.

Fig. 1(b) demonstrates the challenges of applying the method in [14] to the CSI values of all 30 sub-carriers obtained from conventional WiFi devices that use **on-board omnidirectional antenna**. Here, we used a pair of laptops separated by a distance of 1 m. A user was sitting at approximately 0.5 m from the laptops. We directly applied the same method as in [14] to process the data. The thin magenta lines in Fig. 1(b) show the PSD of the sub-carriers and they were significantly noisier than those in Fig. 1(a). The thick blue line shows the mean PSD. The heart rate is then estimated from the peak PSD as in [14] to be 68 bpm, which is significantly different to the ground truth value of 77 bpm. On the other hand, the proposed CardioFi, which will be introduced and discussed in later sections, produced an estimation of 76 bpm (the red line in the figure) that is very closed to the ground truth.

Although the CSI data in Fig. 1(b) is noisy, we can see that the signals contain useful information as the PSD of a number of sub-carriers has a peak close to the actual heart rate. The top circular ticks in Fig. 1(b) depict the positions of sub-carriers' PSD peaks. The opacity of the tick shows the number of sub-carriers with the peak at that position. Anecdotally, six sub-carriers out of thirty differ from the actual heart rate by 0.9 bpm only.

We show another example in Fig. 2, where we track the PSD for each sub-carrier over time. We calculate the peak of the PSD curve for each sub-carrier and use the peaks as heart rate estimates. The lightly shaded area shows the heart rate estimate bounds defined by the minimum and maximum PSD peaks among all sub-carriers. Similarly, the dark shaded area gives a heart rate estimate as bounded by 10% and 90% percentile of individual sub-carrier estimates. Although the range is fairly wide, note the range still includes the actual heart rate shown by the black line which was measured with an external heart rate monitor. We conclude that despite the significant increase in RF noise due to omnidirectional antennas, CSI data contains useful heart rate information. In the next section, we

will present a suite of algorithms that CardioFi uses to filter out the noise and substantially improve accuracy of heart rate estimation from CSI data collected with omnidirectional antennas.
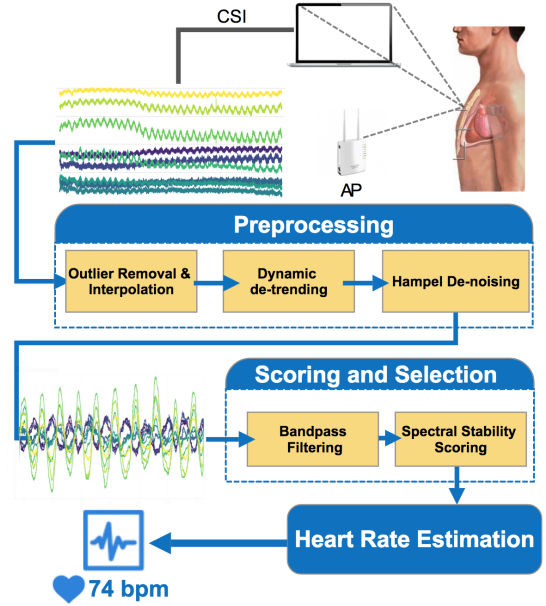
Figure 3: The architecture of CardioFi.

3 CARDIOFI

Fig. 3 shows the architecture of CardioFi, which consists of two WiFi devices. One device acts as the transmitter and the other as the receiver; the receiver is assumed to have multiple antennas, which is common for the WiFi devices nowadays. Fig. 3 depicts the transmitter and the receiver as an access point and a laptop respectively. The transmitter sends packets to the receiver at a regular interval. If a subject is in the vicinity of the devices then this subject's heart beats, as well as other movements, will modulate the wireless signals arriving at the receiver. Therefore, the CSI contains the information of the heart rate of the subject.

The receiver continuously records the CSI of the received packets in different sub-carriers. The CSI data is used to compute the phase difference (PD) between the antenna pairs. In the first stage, CardioFi preprocesses the PD data using outliers removal and noise filtering algorithms. The second stage constitutes a key technical contribution of this paper, where we use novel algorithms to score and select sub-carriers that are the most informative to heart rate. In the last stage, data fusion is used to fuse information from the top scored sub-carriers to produce the final heart rate estimate.

3.1 Background

The physical layer of the latest WiFi standard is based on the Orthogonal Frequency Division Multiplexing (OFDM) modulation technique. OFDM uses a number of orthogonal sub-carriers and transmits data independently on each of the sub-carriers. Assuming there are m transmit antennas and n receive antennas, the CSI of all data streams can be expressed as:

$$\begin{pmatrix} H_{1,1} & H_{1,2} & \cdots & H_{1,n} \\ H_{2,1} & H_{2,2} & \cdots & H_{2,n} \\ \vdots & \vdots & \ddots & \vdots \\ H_{m,1} & H_{m,2} & \cdots & H_{m,n} \end{pmatrix} \quad (1)$$

where $H_{i,j}$ is the CSI vector between the i-th transmit antenna and the j-th receive antenna. Commodity WiFi cards make the CSI of some of the sub-carriers available, e.g. Intel 5300 WiFi cards can export the CSI of 30 sub-carriers. Let C denote the number of sub-carriers whose CSI is available, then each $H_{i,j}$ is a vector with C elements. We use H to denote a generic $H_{i,j}$ and we write:

$$H = [h_1, h_2, \cdots, h_C] \quad (2)$$

where h_i denotes the CSI for sub-carrier i in the CSI vector H. The CSI h_i is a complex number which combines the effect of attenuation, reflection and scattering of the radio sub-carriers when they propagate from the transmitter antenna to the receiver antenna. The CSI can be expressed in terms of the multi-path attributes. Assuming that the radio propagation in h_i (whose frequency is f_i) is the combined effect of P multi-paths where the attenuation and propagation delay on the k-th path (where $k = 1, \ldots, P$) are denoted by respectively, p_k and τ_k, then we can write:

$$h_i = \sum_{k=1}^{P} p_k e^{-j2\pi f_i \tau_k} \quad (3)$$

In our context, some of the multi-paths may be modulated by the movement of the heart of a subject, see Fig. 3, and these multi-paths provide information on the heart rate of the subject.

Instead of using CSI h_i, one may also use the magnitude and phase of h_i to infer the information on the heart rate. However, a challenge of using the phase of h_i obtained from COTS WiFi devices is that there is an unknown random offset in the phase measurements which varies from packet to packet. Fortunately, this unknown offset is the same for multiple receiving antennas for a given packet [29]. This is because the antennas are on the same Network Interface Card (NIC) and hence they use the same system clock and the same down-converter frequency. Therefore, it is possible to remove this unknown offset by subtracting the phase measurements from two receiving antennas. Hence, CardioFi uses the phase difference (PD) as the raw data for the heart rate estimation.

3.2 Preprocessing

The preprocessing stage consists of three sub-steps: outlier removal, de-trending and de-nosing, see Fig. 3. The input to the preprocessing block is the PD of all sub-carriers and the preprocessing is done for each individual sub-carrier independently.

The removal of outliers is performed by a Hampel filter. We begin by computing the median μ and the mean absolute deviation σ over a time window (T_1) of the PD data. By using a threshold τ_1, we discard the data that lie outside the interval $[\mu - \tau_1 \times \sigma, \mu + \tau_1 \times \sigma]$. CardioFi chooses T_1 to be 0.5 seconds and τ_1 to be 0.4. Then, linear interpolation is performed to maintain uniform sampling (due to interference caused by other devices in the same WiFi channel, packets received may not be evenly distributed in time).

The next step is to remove the trend in the data. This step is important because we observed during our experimentation that sub-carriers could go through unpredictable abrupt changes, see Fig. 4(a). These changes could occur when the user made sudden movements and they appeared in all sub-carriers.

Since the abrupt changes in PD can last for a short time or a long period of time, see Fig. 4(a), we propose a de-trending method called **Dynamic Window** (DW). The basic idea of DW is to divide the PD time series into non-overlapping windows and if de-trending has been correctly performed, we expect the variance in each window to be almost the same. This means that if the trend changes slowly, then we can use a larger window size; and vice versa. The purpose of the DW algorithm is to determine this window size adaptively.

The DW algorithm begins by computing the average variance over c windows where the default window size is used. Let v_w denotes the variance of the w-th window. The DW algorithm computes

$$E_v = \frac{1}{c} \sum_{w=1}^{c} v_w \quad (4)$$

The next step is to determine the size of the next window so that the variance of the data in the next window is almost the same as E_v. We do this by increasing the size of the next window until either the variance of the data in the window exceeds αE_v where α is a parameter or the window size reaches a preset limit of l. In our experiments, we chose $c = 5$, $l = 3$ seconds and $\alpha = 1.2$. Green dashed vertical lines in Fig. 4b(b) depict the dynamic windows.

The advantage of DW algorithm is that it can capture abrupt changes in the signal accurately. We compare the accuracy of the DW algorithm against the Moving Average (MA) method with a fixed window size, see Fig. 4(b)(c). DW-based de-trending clearly performs better than the MA method.

After de-trending, another Hampel filter is used to remove the noise. Fig. 4(d) shows the de-noised data (window size, or T_2, is 0.5 second and τ_2 set to 0.1).

3.3 Sub-carrier Selection

As discussed in Section 2, some sub-carriers are more informative to heart rate estimation. Here we present a method to assess the quality of estimation of each sub-carrier.
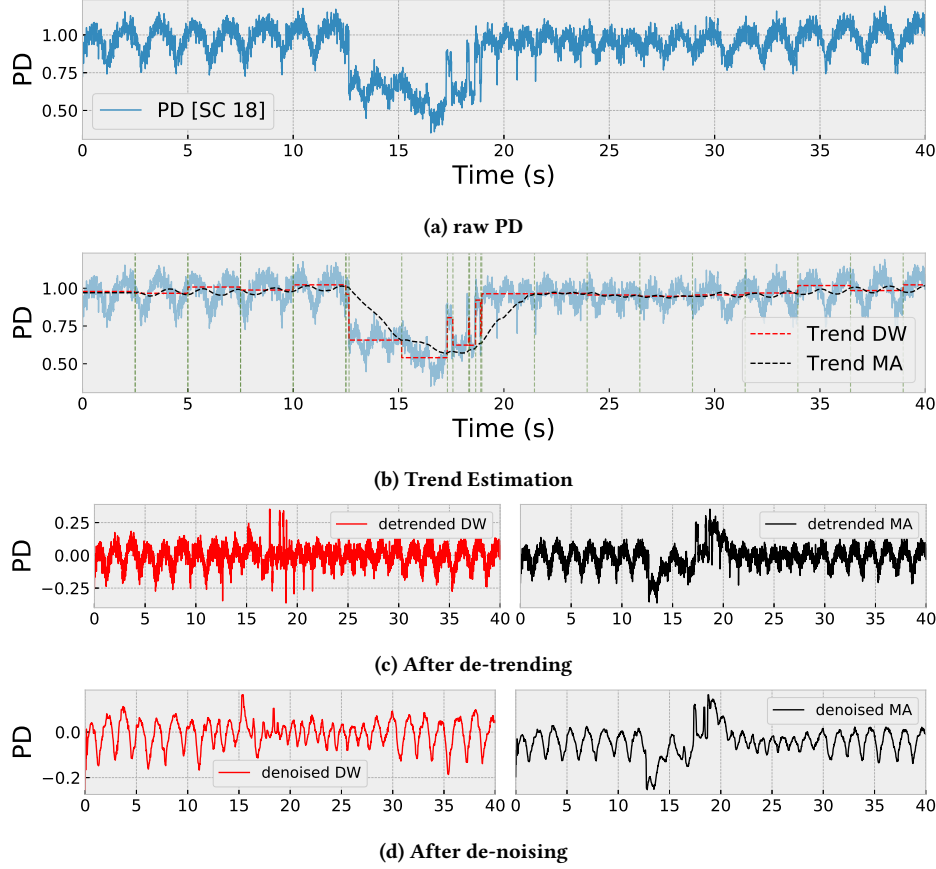
(a) raw PD

(b) Trend Estimation

(c) After de-trending

(d) After de-noising

Figure 4: CardioFi preprocessing

The sub-carrier selection step consists of two sub-steps, see Fig. 3. The first step is to use a bandpass filter to remove the frequency components in which the heart rate is unlikely to be found. Following [20], we retain the frequency in the interval $[\max(2 * BR, 50), 2]$ Hz, where BR is the estimated breathing rate, to avoid the frequency harmonics caused by breathing. The breathing rate is estimated as the frequency component with strongest power in the breathing range. Note that the breathing rates generally range from 0.2-0.5Hz.

The next step is to determine the quality of the sub-carriers. Earlier methods [14, 27] made use of the fact that different sub-carriers have different wavelengths and this difference can result in different sensitivity levels for the motion of interest. Hence, the mean absolute deviation of sub-carriers' signals is used as a quality metric. Generally the larger the deviation is, the higher the sensitivity is.

In this paper, we propose a novel **Spectral Stability** method to determine the quality of the sub-carriers. Our method is based on an observation that the true heart rates do not change rapidly over a short time duration. Therefore, we calculate the heart rate estimate multiple times over a short duration. If the estimates are consistent, then the signal is likely to be of good quality.

In order to calculate the spectral stability score at time t, we consider a time interval of length T_3 and divide the interval $[t - T_3 :$
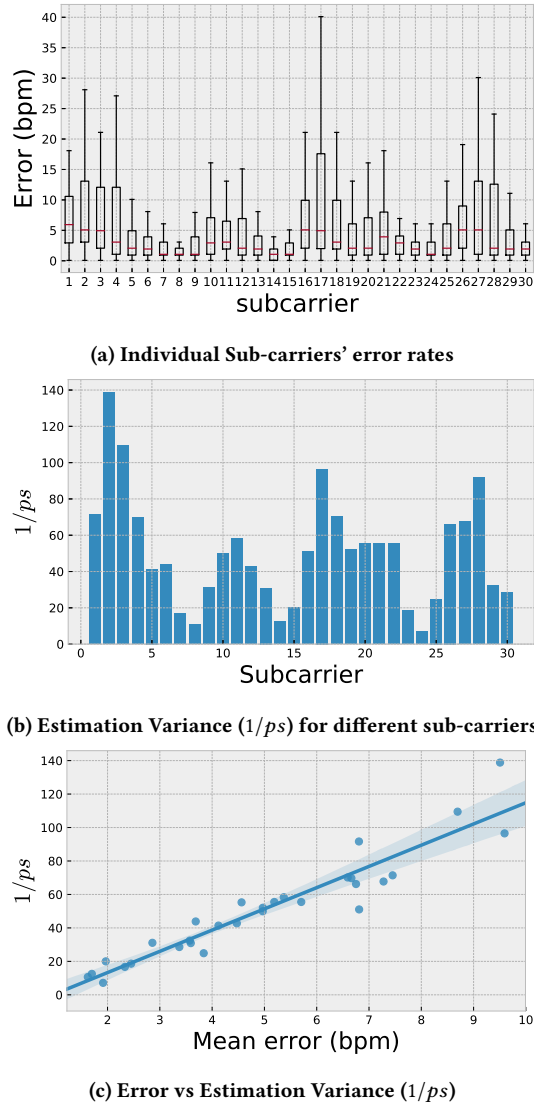
$t]$ into N sliding windows. Each window is w_f[1] seconds long and overlapped by $w_f - 1$ seconds with the following window. For sub-carrier i and time window n (for $n = 1 \ldots N$), we determine the peak frequency of the PD time-series as $r_{i,n}$. The value of $r_{i,n}$ can be considered as one of the heart rate estimates. We define the Spectral Stability score ps_i of sub-carrier i as:

$$ps_i = \frac{1}{\text{variance}(r_{i,1}, \ldots, r_{i,N})} \tag{5}$$

We now demonstrate that the spectral stability score is indeed a good indicator of the quality of the heart rate estimation. We conducted an experiment where we used the individual sub-carriers to estimate the heart rates and the true heart rates are also collected. Fig.5(a) shows the error of the estimated heart rates. It can be seen that there is a lot of variation in the estimation error but some carriers produced low estimation error. Fig.5(b) shows the variance of the estimated heart rates, i.e. the denominator of Eq. (5). Fig.5(c) plots the variance of the estimated heart rates against the error in the estimated heart rates. The figure shows that there is a high correlation between the two quantities, which demonstrates that we can use the spectral stability score to assess the quality of the sub-carriers for the heart rate estimation.

---

[1]The impact of the values of N and w_f will be investigated in Section 4.2.2

(a) Individual Sub-carriers' error rates

(b) Estimation Variance ($1/ps$) for different sub-carriers


(c) Error vs Estimation Variance ($1/ps$)

Figure 5: Correlation between estimation error and the calculated estimation variance ps

Fig. 6 further illustrates the effectiveness of the proposed subcarrier selection scheme. Fig. 6(a) shows the heart rates estimated by using the sub-carrier with the highest spectral stability score. It can be seen that the estimated heart rates (blue curve) follow the actual heart rates (black curve) closely, with a median error of 2.4 bpm only. On the other hand, if we use the sub-carriers that have the largest variance, then the heart rate estimation (green curve) is poor as shown in Fig. 6(b) with a median error of 5.2 bpm which is more than double of that in Fig. 6(a).

3.4 Heart Rate Estimation

After computing the spectral stability score for the sub-carriers, the next step is to use the scores to select the good sub-carriers. We first normalise the spectral stability scores before excluding the

(a)

(b)
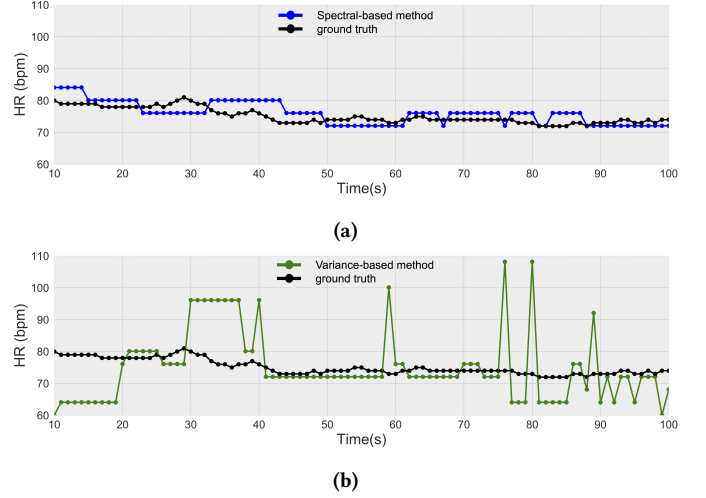
Figure 6: Heart rate estimation from highest scoring subcarrier selected using Spectral-based (a) and Variance-based (b) selection methods.

sub-carriers whose scores are less than 20% of the score of the best sub-carrier. We fuse the data from the most informative sub-carriers by calculating the mean PSD spectrum across the sub-carriers. The final instantaneous heart rate is then estimated as the frequency component with the largest magnitude in the mean PSD spectrum.

The output of the whole processing pipeline for a 200-second segment is shown in Fig. 7(a). The figure shows estimated heart rate from CardioFi and also from [14]. It can be seen that CardioFi tracks the true heart rates very closely. Fig. 7(b) shows the box plot of the estimation errors from CardioFi and [14] respectively. The median error for CardioFi is 1.0 bpm, while that of [14] is 1.9 bpm, which is 90% larger.

Fig. 7(c) and (d) illustrate the performance gap between CardioFi and [14]. They show the estimated spectra of the two methods at time 150 seconds of Fig. 7(a). The behaviour of Fig. 7(c) is similar to that in Fig.1(b) introduced earlier where the estimated spectra are very noisy. However, CardioFi obtained a better spectrum estimation by judiciously choosing the informative sub-carriers using the spectral stability score. Note also that in Fig. 7(d), only 5 sub-carriers were selected.

4 EVALUATION

We evaluated CardioFi in office room and bedroom environments. Fig. 8 illustrates the environments we considered for our experiments, the placements of devices, and the location of a subject.

The first setup (Fig. 8(a)) represents the setup of the contactfree heart rate monitoring for a quasi-static subject (watching TV, reading, etc.). The subject's body does not intersect the line of sight (LoS) between the sender and the receiver. Typical applications include long-term vital sign monitoring for medical applications and instantaneous heart rate monitoring after exercise as postexercise recovery rates were shown to be a strong predictor of mortality [6]. Another example is a subject observing the slowing down of her heart rates in real-time while practicing meditation

(a) Perfomance of CardioFi vs Liu et. al.[14] for 200 seconds segment

(b) Error rate

(c) Mean frequency spectrum at time 150 second of (a) according to [14]

(d) Mean frequency spectrum at time 150 second of (a) as observed by CardioFi
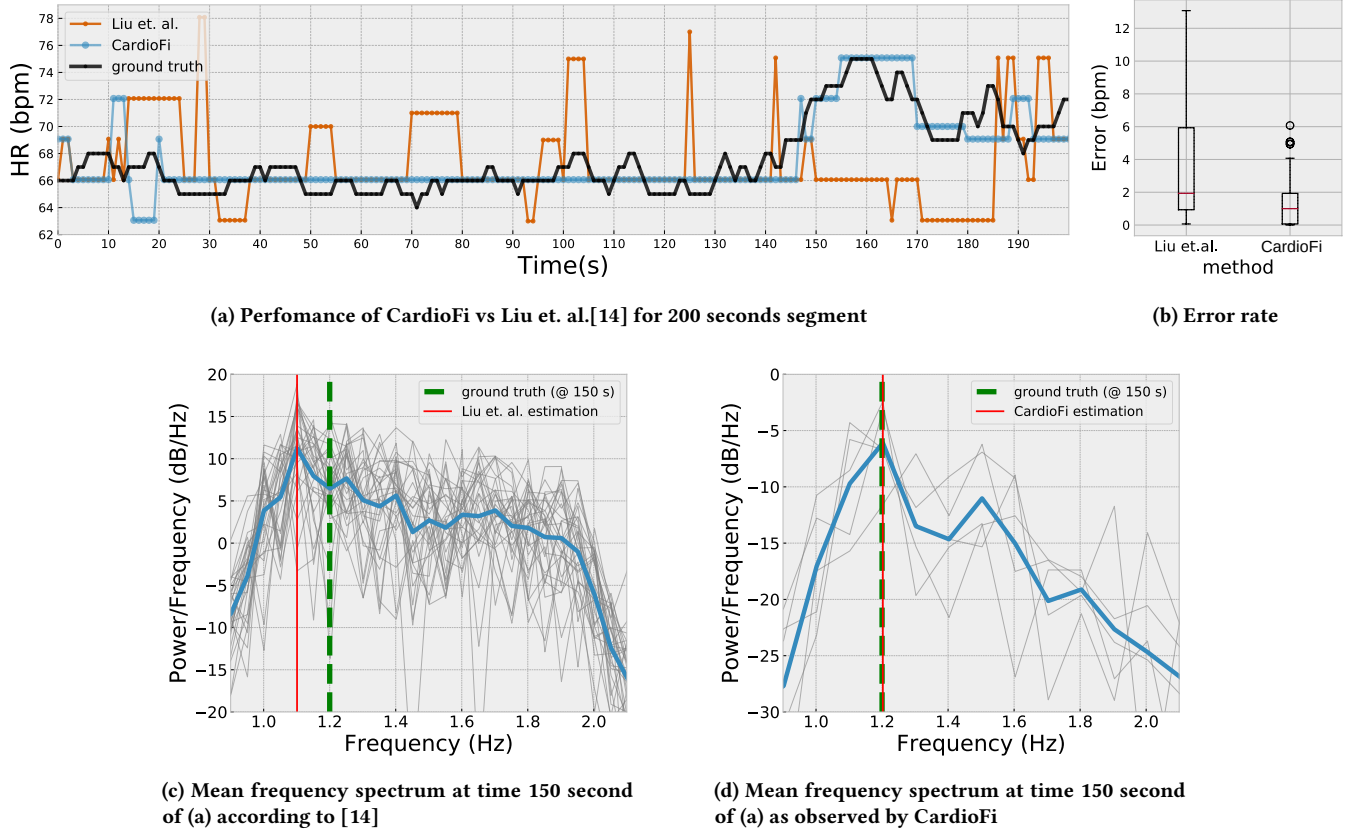
Figure 7: The performance of CardioFi vs that of Liu et. al. [14]

[1]. The second (Fig. 8(b)) setup is a representative environment for the vital sign monitoring during sleep.

The WiFi transmitter and receiver are two HP Elitebook 6930p laptops equipped with Intel 5300 WiFi card and both devices use internal antennas. CSI data was collected using Linux 802.11n CSI Tool [9] in the 5 GHz band. Four volunteers participated in the data collection process over a total period of 2 months[2]. The ground truth for heart rates was collected at 1 Hz by the Polar H7 sensor [2], which was wrapped around the subject's chest and reported the instantaneous heart rates over bluetooth. Network time protocol was used to synchronize the CSI and Polar H7 data streams. We varied the distances between a user and the LoS of devices for different Tx/Rx placement scenarios. Except for the results in Fig. 9(b), the distances were less than 2 m.

4.1 Overall Performance

We begin by evaluating the heart rate estimation of our proposed approach (Fig. 9(a)) and investigate how the performance changes with increasing distance of the user from the WiFi devices.

Compared to the baseline method in [14], CardioFi decreases the median error from 1.9 bpm to 1.14 bpm, a 40% reduction. Moreover, 90% of the errors are below 5.1 bpm which improves the baseline

[2]Data collection was approved by the Human Research Ethics committee in University of New South Wales, Sydney, Australia.

algorithm by 176%. In general, the proposed approach has a median error comparable to device-less systems implemented with directional antennas [14, 28] and device-based accelerometer systems [11]. This is achieved without requiring hardware modifications or direct contact with subject's body.

We next test the impact of increasing the distance between the subject and any of the communicating devices and plot our results in (Fig. 9(b)). As the distance increases, the reflected signal becomes weaker and hence the accuracy degrades gradually until reaching the median error of 1.6 bpm at distance of 2 meters. We find the signal becomes very noisy when the distance goes beyond 2 meters, resulting in a substantial increase of the error. Upon closer inspection of the signal, the majority of the sub-carriers fail to produce accurate estimation of the heart rate, which ultimately leads to large errors in the data fusion stage. We consider only distances up to two meters in the experiments for the rest of this paper.

4.2 Impact of Parameters

4.2.1 Impact of Sub-carrier selection. In this section we study the effect of the sub-carrier selection step on the produced estimation results.

Fig. 10(a) shows the error as we change the number of sub-carriers considered for each criterion. We compare our proposed **Spectral Stability** score to the variance-based sub-carrier selection

(a) Office room setup

(b) Bedroom setup

Figure 8: Experimental setup scenarios

(a) CDFs of heart rate estimation error

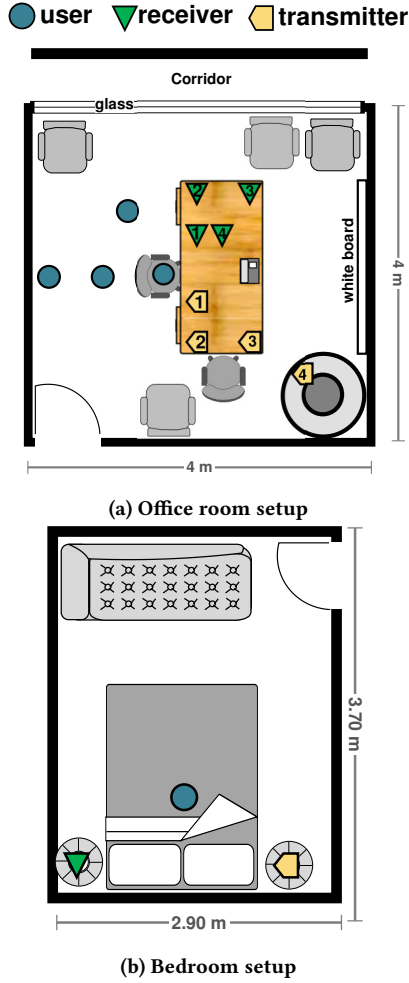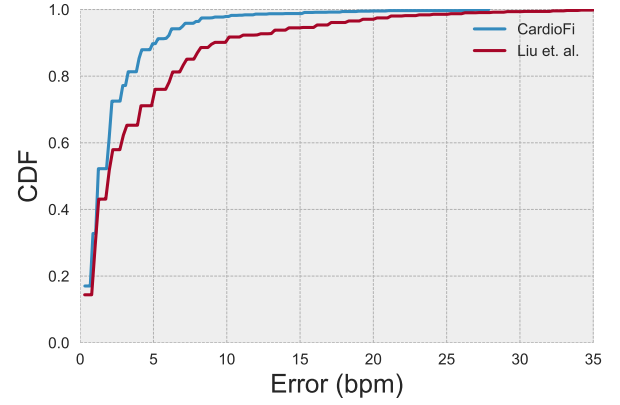**(b) The impact of user-to-device distance on median error**
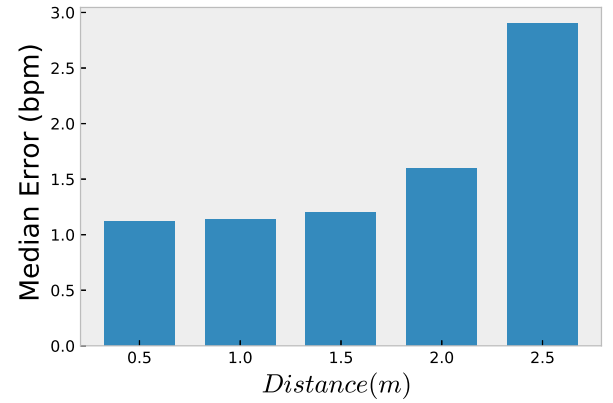
Figure 9: The performance of CardioFi.

schemes in which the sub-carrier score is calculated based on variance of signal itself. The spectral stability method outperforms the variance based method for the top ranked sub-carrier, with 2.8 bpm and 3.14 bpm median error, respectively. The estimation improves as we include more sub-carriers until reaching 10 sub-carriers and the median error of 1.14 bpm and 1.8 bpm for spectral and variance methods, respectively. On average, the spectral stability method decreases the median error of the variance method by 19%.

Second important parameter used in the sub-carrier selection step is the window length N for assessing the spectral stability. Fig. 10(b) illustrates that the median error is insensitive to $N \geq 20$ (median error 1.1 bpm). Smaller N values produce poor spectral stability score (median error 1.4 bpm) as all sub-carriers tend to score close to zero, making it difficult to identify reliable sub-carriers. We set the value of N to be 40 seconds.

4.2.2 Sliding Window Length w_f. The window length used for calculating the FFT balances the need of obtaining accurate results and the initial delay in the system response. Ideally, larger window size is preferred to obtain more accurate results. However,

this comes at the cost of increased computational processing and delayed reporting due to the initial delay. Fig. 10(c) shows that segments as small as 10 seconds are sufficient for obtaining the heart rate with median error of 1.9 bpm. We set the value of w_f to 20 seconds.

4.2.3 Impact of Sampling Rates. Fig. 10(d) shows the median error for different sampling rates. Error ranges (5th-90th percentile) are depicted as the vertical lines. While sampling at 20 samples per second should be theoretically sufficient for capturing the heart rate, we find this rate unreliable in practice. The results show that higher sampling rates reduce median errors. However, this effect diminishes above 100 samples per second. Hence, we set the sampling rate to 100 samples per second in our evaluation.

5 RELATED WORKS

CardioFi is related to a large body of literature concerned with vital sign monitoring. In this section we survey categories of closely related vital sign monitoring research.

As an important indicator for human health condition and stress levels, heart rate is traditionally acquired through **medical** dedicated equipments such as electrocardiography (ECG) or pulse

(a) Number of selected sub-carriers

(b) Spectral Stability window length (N)

(c) Sliding window length (w_f)
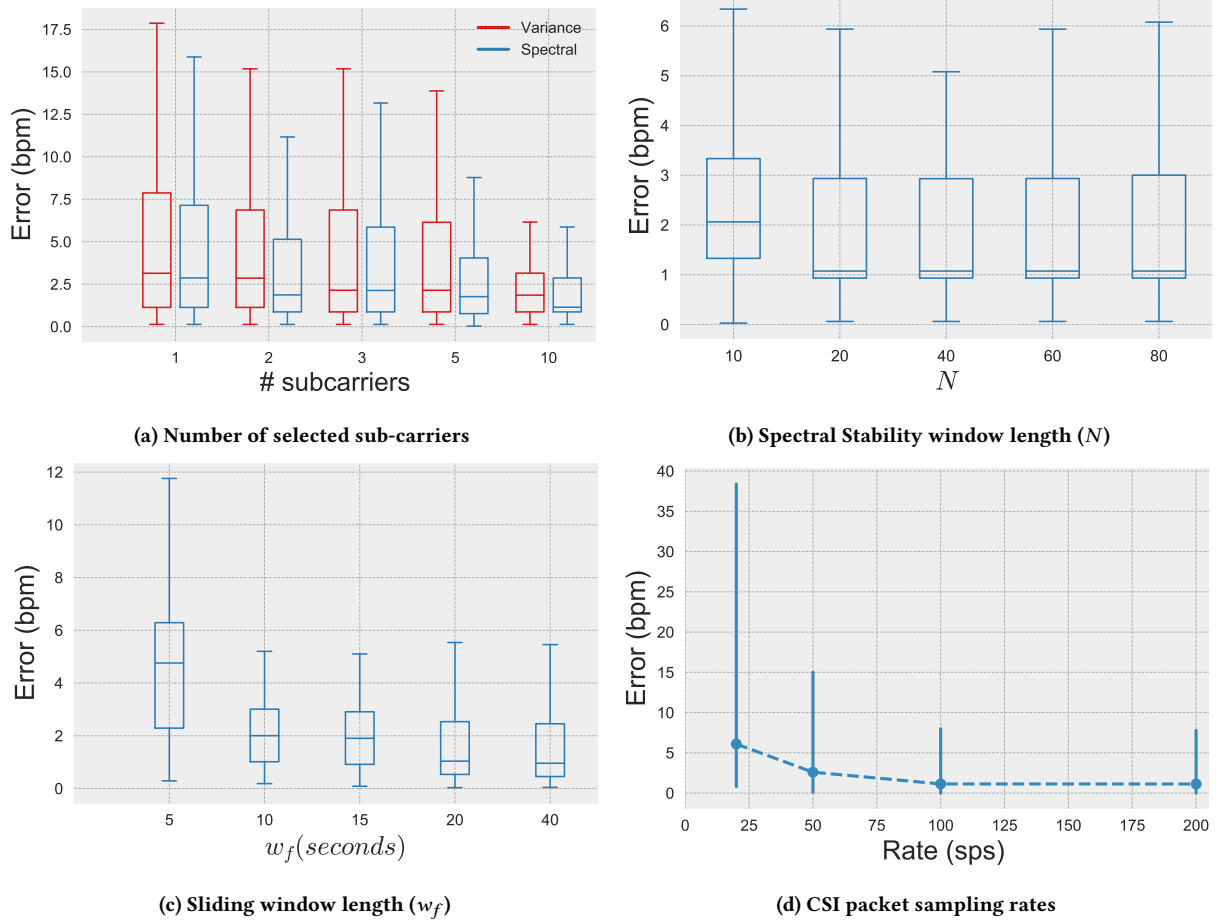
(d) CSI packet sampling rates

Figure 10: The impact of CardioFi parameters

oximeters. Although accurate, the **inconvenience** of wearing them motivated researchers to investigate alternative monitoring techniques, especially for applications that require daily monitoring. The techniques can be generally broken down into two categories: wearable devices and device-free monitoring.

Wearable device monitoring: A large body of previous research assumes that sensors are attached to the user to capture the heart beating rates. Examples include wearable accelerometers that detect tiny heart beating motion [8, 22].To introduce a ubiquitous alternative, smartphones' built-in sensors were employed by a number of systems for vital sign monitoring[3, 11, 13, 19]. LivePulse [10] detects changes in transparency of users' fingertips by the built-in camera of a mobile device to infer the heart rates. Heart-Sense [18] fuses inertial sensors measurements of phone strapped on a subject's chest to obtain her heart rates. These approaches require **contact with the subject's body**, rendering them **uncomfortable** on the long term.

Device free systems: can monitor vital signals of a user without requiring her to wear a sensor. Recently, there has been a number of relevant interesting research efforts. They can be categorized into three groups.

1) Vision contact-less sensing: These techniques, in general, either track changes in color intensity [25, 30], or the tiny body vibration caused by heartbeat [5, 24]. In addition to **privacy concerns**, **illumination conditions affect the performance** of these systems.

2) Acoustic contact-less sensing: Unlike WiFi, separating acoustic signal reflections based on arrival times, which translates to distances range, is feasible due to the significantly lower speed of the sound compared to that of radio. Furthermore, since most systems employ co-located speaker and microphone and use the same frequency, there is no carrier frequency offset (CFO) errors between the sender and the receiver. These advantages were leveraged by many efforts that used smartphones built-in microphone and speaker to convert the phone into active sonar capable of monitoring vital signs. Acousticcardiogram [20] demonstrated the feasibility of obtaining breathing and heart rates. The **limited operational distance (within a few centimeters)** is the main obstacle for the wide adoption of acoustic approaches.

3) Radio contact-less sensing: Radio based sensing systems belong to the most popular device-free systems. [4] uses *T-shaped special antennas* and ultra-wideband FMCW radar to monitor breathing

and heart rate of smart homes occupants. EQ-Radio [35] extends [4] to acquiring Heart Rate Variability (HRV) and uses it for emotion recognition. mmVital [31] uses the Received Signal Strength of the *highly directional 60 GHz millimeter radio signal* for breathing and heart rates monitoring. Liu et. al. [15] leveraged **the amplitude information of CSI** to monitor breathing and heart rates during sleep. PhaseBeat [28] used CSI phase difference for the same purpose. Both [15] and [28] employ **directional antennas** for the heartbeat monitoring scenario to boost the radio signal quality. The main distinction between CardioFi and earlier device-free RF heartbeat monitoring systems is addressing the accurate HR estimation problem on COTS WiFi devices **without relying on hardware enhancement**. We manage to get reliable heart rate estimation by efficient data processing and fusing input from informative subcarriers only. We believe that enabling vital sign monitoring on ubiquitous unmodified WiFi devices is a key enabler of many interesting applications including biofeedback.

6 CONCLUSION

In this paper we presented a system for heart rate monitoring on top of COTS WiFi devices. We showed the challenges of heart beat tracking on consumer grade WiFi systems and addressed them by a novel signal processing pipeline without resorting to noise mitigation hardware (i.e. directional antennas). Our results showed that the proposed CardioFi system outperforms state-of-the-arts by reducing their 50- and 90-th percentile error by 40% and 176%, respectively.

REFERENCES

[1] 2018. Meditation offers significant heart benefits. https://www.health.harvard.edu/heart-health/meditation-offers-significant-heart-benefits [Online; accessed 1-July-2018].
[2] 2018. Polar H7. https://support.polar.com/au-en/support/H7_heart_rate_sensor [Online; accessed 1-July-2018].
[3] Heba Abdelnasser, Khaled A Harras, and Moustafa Youssef. 2015. UbiBreathe: A ubiquitous non-invasive WiFi-based breathing estimator. In *Proceedings of the 16th ACM International Symposium on Mobile Ad Hoc Networking and Computing*. ACM, 277–286.
[4] Fadel Adib, Hongzi Mao, Zachary Kabelac, Dina Katabi, and Robert C Miller. 2015. Smart homes that monitor breathing and heart rate. In *Proceedings of the 33rd annual ACM conference on human factors in computing systems*. ACM, 837–846.
[5] Guha Balakrishnan, Fredo Durand, and John Guttag. 2013. Detecting pulse from head motions in video. In *Computer Vision and Pattern Recognition (CVPR), 2013 IEEE Conference on*. IEEE, 3430–3437.
[6] Christopher R Cole, Eugene H Blackstone, Fredric J Pashkow, Claire E Snader, and Michael S Lauer. 1999. Heart-rate recovery immediately after exercise as a predictor of mortality. *New England journal of medicine* 341, 18 (1999), 1351–1357.
[7] Anne De Groote, Muriel Wantier, Guy Chéron, Marc Estenne, and Manuel Paiva. 1997. Chest wall motion during tidal breathing. *Journal of Applied Physiology* 83, 5 (1997), 1531–1537.
[8] M Di Rienzo, E Vaini, P Castiglioni, G Merati, P Meriggi, G Parati, A Faini, and F Rizzo. 2013. Wearable seismocardiography: Towards a beat-by-beat assessment of cardiac mechanics in ambulant subjects. *Autonomic Neuroscience: Basic and Clinical* 178, 1 (2013), 50–59.
[9] Daniel Halperin, Wenjun Hu, Anmol Sheth, and David Wetherall. 2011. Tool release: Gathering 802.11 n traces with channel state information. *ACM SIGCOMM Computer Communication Review* 41, 1 (2011), 53–53.
[10] Teng Han, Xiang Xiao, Lanfei Shi, John Canny, and Jingtao Wang. 2015. Balancing accuracy and fun: Designing camera based mobile games for implicit heart rate monitoring. In *Proceedings of the 33rd Annual ACM Conference on Human Factors in Computing Systems*. ACM, 847–856.
[11] Javier Hernandez, Daniel J McDuff, and Rosalind W Picard. 2015. Biophone: Physiology monitoring from peripheral smartphone motions. In *Engineering in Medicine and Biology Society (EMBC), 2015 37th Annual International Conference of the IEEE*. IEEE, 7180–7183.
[12] Donny Huang, Rajalakshmi Nandakumar, and Shyamnath Gollakota. 2014. Feasibility and limits of wi-fi imaging. In *Proceedings of the 12th ACM Conference on Embedded Network Sensor Systems*. ACM, 266–279.
[13] E Jonathan and Martin Leahy. 2010. Investigating a smartphone imaging unit for photoplethysmography. *Physiological measurement* 31, 11 (2010), N79.
[14] Jian Liu, Yingying Chen, Yan Wang, Xu Chen, Jerry Cheng, and Jie Yang. 2018. Monitoring Vital Signs and Postures During Sleep Using WiFi Signals. *IEEE Internet of Things Journal* (2018).
[15] Jian Liu, Yan Wang, Yingying Chen, Jie Yang, Xu Chen, and Jerry Cheng. 2015. Tracking vital signs during sleep leveraging off-the-shelf wifi. In *Proceedings of the 16th ACM International Symposium on Mobile Ad Hoc Networking and Computing*. ACM, 267–276.
[16] Xuefeng Liu, Jiannong Cao, Shaojie Tang, and Jiaqi Wen. 2014. Wi-Sleep: Contactless sleep monitoring via WiFi signals. In *Real-Time Systems Symposium (RTSS), 2014 IEEE*. IEEE, 346–355.
[17] Pedro Melgarejo, Xinyu Zhang, Parameswaran Ramanathan, and David Chu. 2014. Leveraging directional antenna capabilities for fine-grained gesture recognition. In *Proceedings of the 2014 ACM International Joint Conference on Pervasive and Ubiquitous Computing*. ACM, 541–551.
[18] Reham Mohamed and Moustafa Youssef. 2017. HeartSense: Ubiquitous Accurate Multi-Modal Fusion-based Heart Rate Estimation Using Smartphones. *Proceedings of the ACM on Interactive, Mobile, Wearable and Ubiquitous Technologies* 1, 3 (2017), 97.
[19] Panagiotis Pelegris, K Banitsas, T Orbach, and Kostas Marias. 2010. A novel method to detect heart beat rate using a mobile phone. In *Engineering in Medicine and Biology Society (EMBC), 2010 Annual International Conference of the IEEE*. IEEE, 5488–5491.
[20] Kun Qian, Chenshu Wu, Fu Xiao, Yue Zheng, Yi Zhang, Zheng Yang, and Yunhao Liu. 2018. Acousticcardiogram: Monitoring Heartbeats using Acoustic Signals on Smart Devices. (2018).
[21] G Ramachandran and M Singh. 1989. Three-dimensional reconstruction of cardiac displacement patterns on the chest wall during the P, QRS and T-segments of the ECG by laser speckle inteferometry. *Medical and Biological Engineering and Computing* 27, 5 (1989), 525–530.
[22] Ghufran Shafiq and Kalyana C Veluvolu. 2014. Surface chest motion decomposition for cardiovascular monitoring. *Scientific reports* 4 (2014), 5093.
[23] Sheng Tan and Jie Yang. 2016. WiFinger: leveraging commodity WiFi for fine-grained finger gesture recognition. In *Proceedings of the 17th ACM International Symposium on Mobile Ad Hoc Networking and Computing*. ACM, 201–210.
[24] Sergey Tulyakov, Xavier Alameda-Pineda, Elisa Ricci, Lijun Yin, Jeffrey F Cohn, and Nicu Sebe. 2016. Self-adaptive matrix completion for heart rate estimation from face videos under realistic conditions. In *Proceedings of the IEEE Conference on Computer Vision and Pattern Recognition*. 2396–2404.
[25] Neal Wadhwa, Michael Rubinstein, Frédo Durand, and William T Freeman. 2013. Phase-based video motion processing. *ACM Transactions on Graphics (TOG)* 32, 4 (2013), 80.
[26] Guanhua Wang, Yongpan Zou, Zimu Zhou, Kaishun Wu, and Lionel M Ni. 2016. We can hear you with wi-fi! *IEEE Transactions on Mobile Computing* 15, 11 (2016), 2907–2920.
[27] Hao Wang, Daqing Zhang, Junyi Ma, Yasha Wang, Yuxiang Wang, Dan Wu, Tao Gu, and Bing Xie. 2016. Human respiration detection with commodity wifi devices: do user location and body orientation matter?. In *Proceedings of the 2016 ACM International Joint Conference on Pervasive and Ubiquitous Computing*. ACM, 25–36.
[28] Xuyu Wang, Chao Yang, and Shiwen Mao. 2017. PhaseBeat: Exploiting CSI phase data for vital sign monitoring with commodity WiFi devices. In *Distributed Computing Systems (ICDCS), 2017 IEEE 37th International Conference on*. IEEE, 1230–1239.
[29] Xuyu Wang, Chao Yang, and Shiwen Mao. 2017. TensorBeat: Tensor decomposition for monitoring multi-person breathing beats with commodity WiFi. *arXiv preprint arXiv:1702.02046* (2017).
[30] Hao-Yu Wu, Michael Rubinstein, Eugene Shih, John Guttag, Frédo Durand, and William Freeman. 2012. Eulerian video magnification for revealing subtle changes in the world. (2012).
[31] Zhicheng Yang, Parth H Pathak, Yunze Zeng, Xixi Liran, and Prasant Mohapatra. 2016. Monitoring vital signs using millimeter wave.. In *MobiHoc*. 211–220.
[32] Zheng Yang, Zimu Zhou, and Yunhao Liu. 2013. From RSSI to CSI: Indoor localization via channel response. *ACM Computing Surveys (CSUR)* 46, 2 (2013), 25.
[33] J. Zhang, B. Wei, W. Hu, and S. S. Kanhere. 2016. WiFi-ID: Human Identification Using WiFi Signal. In *2016 International Conference on Distributed Computing in Sensor Systems (DCOSS)*. 75–82. https://doi.org/10.1109/DCOSS.2016.30
[34] Jin Zhang, Weitao Xu, Wen Hu, and Salil Kanhere. 2017. WiCare: Towards In-Situ Breath Monitoring. In *14th EAI International Conference on Mobile and Ubiquitous Systems: Computing, Networking and Services (MOBIQUITOUS)*. ACM. https://doi.org/10.4108/eai.7-11-2017.2274069
[35] Mingmin Zhao, Fadel Adib, and Dina Katabi. 2016. Emotion recognition using wireless signals. In *Proceedings of the 22nd Annual International Conference on Mobile Computing and Networking*. ACM, 95–108.